Available online at www.sciencedirect.com
ScienceDirect
International Journal of Heat and Mass Transfer 50 (2007) 1781–1789
International Journal of HEAT and MASS TRANSFER
www.elsevier.com/locate/ijhmt

New scaling of turbulence statistics for incompressible thermal channel flow with different total heat flux gradients

Youhei Morinishi *, Shinji Tamano, Eisuke Nakamura

Graduate School of Engineering, Nagoya Institute of Technology, Gokiso-cho, Showa-ku, Nagoya, Aichi 466-8555, Japan

Received 17 May 2006; received in revised form 27 September 2006
Available online 14 December 2006

Abstract

The scaling of turbulence statistics for wall-bounded thermal turbulent flow with different total heat flux gradients was investigated using direct numerical simulation (DNS) of an incompressible turbulent channel flow with passive scalar transport at the friction Reynolds number of 300 and the Prandtl number of 0.72. DNSs for four cases were performed, where the non-dimensional total heat flux gradients were −1, −0.5, 0 and +0.5. It was revealed that temperature variance and turbulent heat flux were well scaled by the local friction temperature. In addition, using the linear stress-heat flux model, it was shown that the appearance of the logarithmic temperature profile was attributed to the distribution of the turbulent Prandtl number.

Keywords: Direct numerical simulation; Thermal channel flow; Total heat flux gradient; Local friction temperature; Linear stress-heat flux model

1. Introduction

The study on turbulent transport of heat as a passive scalar is attractive from a scientific point of view, and its understanding is of great importance in many engineering applications such as heat exchangers and gas turbines. In particular, the investigation into the effect of different thermal boundary conditions on turbulence statistics is essential to predict the heat transfer from the thermal wall correctly. Therefore, many experimental and numerical studies have been conducted in order to clarify the fundamental mechanism in a wall-bounded incompressible turbulent flow with passive scalar transport. With the increasing performance of the parallel computer, direct numerical simulation (DNS) has played an important role in investigating the detailed mechanism of a wall-bounded incompressible turbulent flow with heat transfer. The DNS of an incompressible turbulent channel flow with passive scalar transport has been extensively studied and provided information valuable in both space and time for the modeling of the wall-bounded turbulent flow with heat transfer [1–13].

In spite of the many DNSs of the incompressible turbulent channel flows with passive scalar transport, the effects of total heat flux gradient β_θ on turbulence statistics have not been well understood. In this study, DNS has been performed to investigate the effects of β_θ on turbulence statistics in the incompressible turbulent channel flows with passive scalar transport. To this end, we performed DNS for Cases 1, 2, 3 and 4, where the non-dimensional wall-normal gradients of the total heat flux β_θ, which was defined in Section 2, were −1, −0.5, 0 and +0.5, respectively. The profiles of turbulence statistics are arranged according to the heat flux gradient, and the new scaling using the local friction temperature is proposed. In addition, the mean velocity and temperature laws are analyzed with the aid of the linear stress and heat flux models.

2. Problem description

The subject of our investigation is the fully developed thermal channel flow between flat parallel walls as show

* Corresponding author. Tel.: +81 52 735 5346; fax: +81 52 735 5442.
E-mail address: youhei.morinishi@nitech.ac.jp (Y. Morinishi).

0017-9310/$ - see front matter © 2006 Elsevier Ltd. All rights reserved.
doi:10.1016/j.ijheatmasstransfer.2006.10.012

in Fig. 1. The flow field is governed by the continuity and Navier–Stokes equations for incompressible flow without the buoyancy effect

$$\frac{\partial u_j}{\partial x_j} = 0, \tag{1}$$

$$\frac{\partial u_i}{\partial t} + u_j \frac{\partial u_i}{\partial x_j} = -\frac{1}{\rho}\frac{\partial p}{\partial x_i} + \nu \frac{\partial^2 u_i}{\partial x_j x_j} - \frac{1}{\rho}\frac{\mathrm{d}P}{\mathrm{d}x_1}\delta_{i1}, \tag{2}$$

where the italic indices i, j, k are obeyed by the convention of summation. In Eqs. (1) and (2), u_i ($i = 1, 2, 3$), p, ρ, and $\nu = \mu/\rho$ are velocity components in the x_i direction, pressure, density, and kinematic viscosity, respectively, where μ is the molecular viscosity. In this paper, x_1, x_2 and x_3 directions are streamwise, wall-normal and spanwise, respectively. In Eq. (2), $\mathrm{d}P/\mathrm{d}x_1$ is the mean pressure gradient. In addition to the flow field, the governing equation of passive scalar $\theta = T - T_l$, where T is the temperature and the subscript l represents the value at the lower wall, is as follows:

$$\frac{\partial \theta}{\partial t} + u_j \frac{\partial \theta}{\partial x_j} = \frac{\kappa}{\rho c_\mathrm{p}} \frac{\partial^2 \theta}{\partial x_j x_j} + Q, \tag{3}$$

where c_p, κ and Q are the specific heat at constant pressure, thermal conductivity and homogeneous internal heat source, respectively.

In a fully developed thermal plane channel flow, the total shear stress and heat flux gradients are balanced with the mean pressure gradient and the internal heat source, respectively

$$\frac{\mathrm{d}\tau_\mathrm{total}}{\mathrm{d}x_2} = \frac{\mathrm{d}P}{\mathrm{d}x_1}, \quad \tau_\mathrm{total} = \tau^\ell + \tau^t = \mu\frac{\mathrm{d}\langle u_1\rangle}{\mathrm{d}x_2} - \rho\langle u_1' u_2'\rangle, \tag{4}$$

$$\frac{\mathrm{d}q_\mathrm{total}}{\mathrm{d}x_2} = \rho c_\mathrm{p} Q, \quad q_\mathrm{total} = q^\ell + q^t = -\kappa\frac{\mathrm{d}\langle\theta\rangle}{\mathrm{d}x_2} + \rho c_\mathrm{p}\langle\theta' u_2'\rangle, \tag{5}$$

where $\langle\ \rangle$ and $'$ represent the Reynolds average (over time and x_1–x_3 plane) and deviation, respectively. The wall boundary conditions for the velocity and temperature are given so as to satisfy Eqs. (4) and (5).

Eqs. (1)–(3) are normalized by using the friction velocity $u_\tau = \sqrt{\tau_w/\rho}$, the friction temperature $\theta_\tau = -q_w/\rho c_\mathrm{p} u_\tau$ and the channel half width H, where τ_w and q_w are the shear stress and heat flux at the lower wall ($x_2 = -H$), respectively, so that the non-dimensional continuity, Navier–Stokes and passive scalar equations are

$$\frac{\partial u_j^+}{\partial x_j^*} = 0, \tag{6}$$

$$\frac{\partial u_i^+}{\partial t^*} + u_j^+ \frac{\partial u_i^+}{\partial x_j^*} = -\frac{\partial p^+}{\partial x_i^*} + \frac{1}{Re_\tau}\frac{\partial^2 u_i^+}{\partial x_j^* x_j^*} - \beta\delta_{i1}, \tag{7}$$

$$\frac{\partial \theta^+}{\partial t^*} + u_j^+ \frac{\partial \theta^+}{\partial x_j^*} = \frac{1}{PrRe_\tau}\frac{\partial^2 \theta^+}{\partial x_j^* x_j^*} - \beta_\theta, \tag{8}$$

where $t^* = tu_\tau/H$ and $x_j^* = x_j/H (j = 1, 2, 3)$. The superscript $+$ represents the variable normalized by u_τ, θ_τ and ρ. The friction Reynolds and Prandtl numbers are defined as $Re_\tau = u_\tau H/\nu$ and $Pr = c_\mathrm{p}\mu/\kappa$, respectively. The non-dimensional total shear stress gradient is defined as $\beta = (H/\rho u_\tau^2)(\mathrm{d}\tau_\mathrm{total}/\mathrm{d}x_2) = (H/\rho u_\tau^2)(\mathrm{d}P/\mathrm{d}x_1)$ and is -1 for the plane channel flow. The non-dimensional total heat flux gradient is defined as $\beta_\theta = -(H/\rho c_\mathrm{p} u_\tau\theta_\tau)(\mathrm{d}q_\mathrm{total}/\mathrm{d}x_2) = -QH/u_\tau\theta_\tau$. Note that the thermal flow is classified by using β_θ as shown in Eq. (8). In fact, this gives the general extension of the classification by Teitel and Antonia [5]. Note that the minus sign appearing in the definition of β_θ is introduced on the analogy of the velocity field and the definition of heat flux, $q_j = -\kappa\mathrm{d}\theta/\mathrm{d}x_j$.

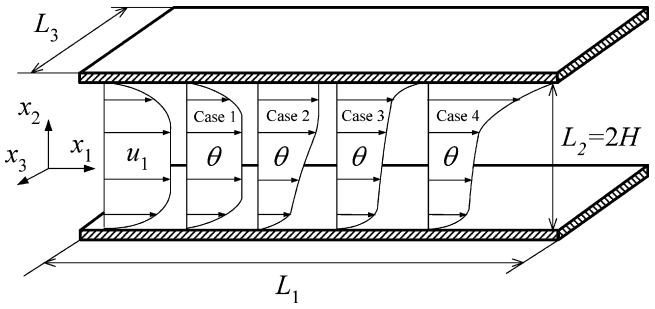

Fig. 1. Thermal plane channel flow.

3. Numerical methods and conditions

Basic equations for the present DNS of the thermal channel flow are Eqs. (6)–(8). As the discrete method in space, the Chebyshev-tau method is used in the wall-normal direction, and the Fourier pseudo-spectral method is used in the streamwise and spanwise directions. The continuity and Navier–Stokes equations are solved simultaneously with the modified Kleiser–Schumann method [14,15]. The skew-symmetric form for convection term is used in Eqs. (7) and (8) for stable long-term integration (see ref. [16]). The semi-implicit time marching algorithm is used in Eqs. (7) and (8) where the diffusion term is treated implicitly with the Crank–Nicolson method, and a third order Runge–Kutta scheme is used for all other terms [17,18]. To solve the discrete Helmholtz equation of the Chebyshev-tau coefficient, the quasi-tri-diagonal matrix solver developed by Canuto et al. [19] was used.

In this study, we consider four computational cases with the no-slip velocity wall boundary condition, which are classified by the non-dimensional total heat flux gradient β_θ. The computational cases are summarized in Table 1. The Reynolds and Prandtl numbers are fixed at $Re_\tau = 300$ and $Pr = 0.72$, respectively. The total shear stress gradient $\beta = -1$ means that the upper and lower walls are stationary, and the flow is driven by the mean pressure gradient. The upper and lower walls for Cases 1, 2, 3 and 4 are isothermal. The values of temperature difference between upper and lower walls, $\Delta\theta^+ = \theta_u^+ - \theta_l^+$, which are given to realize the corresponding β_θ values, are also shown in Table 1. The profiles of the non-dimensional total

Table 1
Computational cases

Case	Re_τ	Pr	β	β_θ	$\Delta\theta^+$
Case 1	300	0.72	−1	−1	0
Case 2	300	0.72	−1	−0.5	22.4
Case 3	300	0.72	−1	0	44.5
Case 4	300	0.72	−1	+0.5	66.3

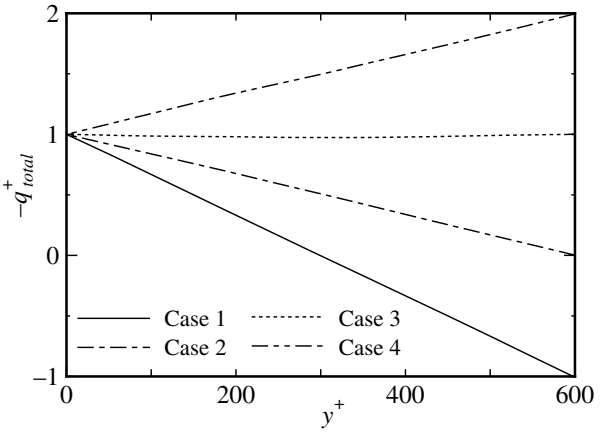

Fig. 2. Profiles of total heat flux.

heat flux, $-q^+_{\text{total}}(= -\langle u_2'^+\theta'^+\rangle + \mathrm{d}\langle\theta\rangle/\mathrm{d}y^+/Pr)$, are shown in Fig. 2. The wall unit is defined as $y^+ = y/\delta_v$, where $y = x_2 + H$ is the distance from the lower wall and $\delta_v = \nu/u_\tau$ is the viscous length scale. Computed total heat flux gradients for Cases 1, 2, 3 and 4 agree well with the given β_θ values, −1, −0.5, 0 and +0.5, respectively. Note that Case 3 corresponds to the incompressible turbulent channel flow between isothermal and adiabatic walls [20,21].

The initial conditions of the present simulations are as follows. The mean streamwise velocity is given by superimposing random velocity fluctuations upon the profile based on Spalding's law [22]. The wall-normal and spanwise velocities are given by random velocity fluctuations with zero mean values, while the plane-averaged velocity fluctuation intensities are given by functions of the wall-normal coordinate and go to zero at the wall. The temperature fluctuation is zero, and the mean value is given by an appropriate second polynomial function for each case.

For all cases, grid spacings in the periodic directions (x_1 and x_3 directions) are uniform, and the wall-normal grids are given by Gauss–Lobatto points [19]. The computational domain size ($L_1 \times L_2 \times L_3$), number of grid points ($N_1 \times N_2 \times N_3$), and grid width in wall units ($\Delta x_1^+ \times \Delta x_2^+ \times \Delta x_3^+$) are given in Table 2. The grid resolution

Table 2
Grid resolution

$L_1 \times L_2 \times L_3$	$L_1^+ \times L_2^+ \times L_3^+$	$N_1 \times N_2 \times N_3$	$\Delta x_1^+ \times \Delta x_2^+ \times \Delta x_3^+$
$2\pi H \times 2H \times 2\pi H/3$	$1885 \times 600 \times 628$	$128 \times 161 \times 128$	$15 \times (0.058\text{–}5.9) \times 4.9$

is evaluated by $\Delta x_i^+ = \Delta x_i/\delta_v (i = 1, 2, 3)$, where Δx_i is the grid spacing in the x_i direction. It is shown that the present spatial resolution is comparable or better than that of previous DNS attempts for the corresponding incompressible turbulent channel flow with the same spatial discretization method (spectral). It is verified that the present DNS data had sufficient resolution and domain size by examining one-dimensional energy spectra and two-point correlations (not shown here).

The present turbulence statistics are obtained by averaging over space (x_1 and x_3 directions) and time of $20H/u_\tau$ after the turbulent flow becomes stationary, where the time increment $\Delta t/(H/u_\tau)$ is 0.0004. The code verification is done in the thermal channel flow of cases corresponding to Case 1 ($\beta = -1$, $\beta_\theta = -1$) and Case 3 ($\beta = -1$, $\beta_\theta = 0$) at the Reynolds number of 150 and the Prandtl number of 0.72 (see [21]). Note that DNSs for Case 2 ($\beta = -1$, $\beta_\theta = -0.5$) and Case 4 ($\beta = -1$, $\beta_\theta = +0.5$) have not been done as far as we know.

4. Results and discussion

4.1. Mean velocity and temperature profiles

The mean velocity scaled by the friction velocity, $\langle u_1\rangle^+ = \langle u_1\rangle/u_\tau$, and the mean temperature scaled by the friction temperature, $\langle\theta\rangle^+ = \langle\theta\rangle/\theta_\tau$, are shown in Fig. 3, where the abscissa is the wall unit from the lower wall. The mean velocity $\langle u_1\rangle^+$ agrees well with the corresponding DNS data of Iwamoto et al. [24] at $Re_\tau = 300$, in which the simulation was carried out using the same spatial discretization method. The profiles of $\langle\theta\rangle^+$ at $y^+ < 20$ for all the cases are identical. However, the mean temperature scaled by the wall variables increases with increasing β_θ on the lower wall side.

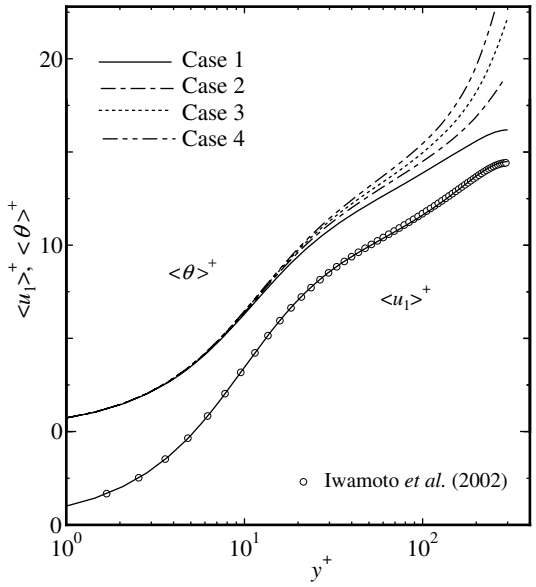

Fig. 3. Profiles of mean velocity and temperature in wall units.

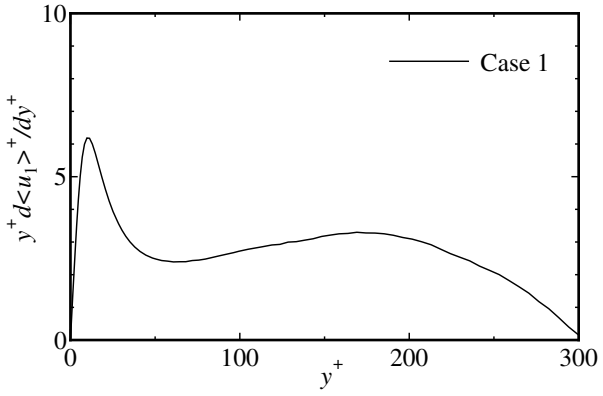

Fig. 4. Inspection of the logarithmic law of mean velocity: $y^+\mathrm{d}\langle u_1\rangle^+\mathrm{d}y^+$.

First, the profile of $y^+\mathrm{d}\langle u_1\rangle^+/\mathrm{d}y^+$ is shown in Fig. 4 to investigate the logarithmic law of the mean velocity. The logarithmic regions of the velocity correspond to the regions where $y^+\mathrm{d}\langle u_1\rangle^+/\mathrm{d}y^+$ is constants. No apparent logarithmic region of velocity is found, and the well-known bump appears around $y^+ \simeq 200$. This is explained by the linear stress model proposed by Townsend [23] for the analysis of mean velocity profile of an equilibrium boundary layer. In a turbulent region ($\tau^t \gg \tau^\ell$), the total shear stress profile is supposed to be linear as $\tau_{\text{total}} = \rho u_\tau^2 + y\mathrm{d}\tau_{\text{total}}/\mathrm{d}y$, where $\mathrm{d}\tau_{\text{total}}/\mathrm{d}y$ is a constant total shear stress gradient. With the aid of the mixing length assumption, $(\tau^t/\rho)^{1/2} = \ell\mathrm{d}\langle u_1\rangle/\mathrm{d}y$ and $\ell = \kappa y$, the mean velocity gradient is written as follows:

$$\frac{\mathrm{d}\langle u_1\rangle}{\mathrm{d}y} = \frac{u_\tau}{\kappa}\frac{(1+\beta y/H)^{1/2}}{y}. \tag{9}$$

Although the above equation is integrable [23], we make use of Eq. (9) for the analysis of the mean velocity law. For instance, the logarithmic law for the mean velocity, $\langle u_1\rangle^+ = (1/\kappa)\log y^+ + B$, is derived from Eq. (9) provided that $|\beta y/H| \ll 1$. As following the above analysis, the logarithmic law for the velocity appears in the region of $|\beta y/H| \ll 1$, which is identical to $y^+ \ll Re_\tau$ with $\beta = -1$, where the wall unit y^+ at the center of the channel corresponds to the Reynolds number Re_τ in this study. This is why the apparent logarithmic region does not appear on the mean velocity profile of the standard (pure Poiseuille, $\beta = -1$) plane channel flow at $Re_\tau = 300$. In addition, employing the expansion, $(1+x)^\alpha = 1 + \alpha x + \alpha(\alpha-1)x^2/2! + \alpha(\alpha-1)(\alpha-2)x^3/3! + \cdots$, Eq. (9) is rewritten as

$$\frac{\mathrm{d}\langle u_1\rangle}{\mathrm{d}y} = \frac{u_\tau}{\kappa}\frac{1}{y}\left[1 + \frac{1}{2}\beta\frac{y}{H} - \frac{1}{8}\beta^2\left(\frac{y}{H}\right)^2 + \cdots\right]. \tag{10}$$

The existence of additional second and higher terms explains the appearance of the bump in Fig. 4. The leading order of the additional term is $O((y/H)^1)$, which strongly restricts the upper bound of the logarithmic region. It also supports the fact observed in a Poiseuille pipe flow experiment [25] ($Re_\tau = 9000$) that the logarithmic law appears in the region of $y^+ < 0.07Re_\tau$.

Second, the profile of $y^+\mathrm{d}\langle\theta\rangle^+/\mathrm{d}y^+$ is shown in Fig. 5 to investigate the logarithmic law of the mean temperature. The logarithmic region of temperature seems to appear only for Case 1. In order to analyze the mean temperature law, we introduce the linear stress-heat flux model, which is an extension of the linear stress model [23]. In a turbulent region ($q^t \gg q^\ell$), the total heat flux is supposed to be linear as $q_{\text{total}} = -\rho c_{\text{p}} u_\tau \theta_\tau + y\,\mathrm{d}q_{\text{total}}/\mathrm{d}y$, where $\mathrm{d}q_{\text{total}}/\mathrm{d}y$ is a constant total heat flux gradient. The mixing length assumption for the turbulent heat flux is $q^t = -\rho c_{\text{p}}(\tau^t/\rho)^{1/2}\ell_\theta\mathrm{d}\langle\theta\rangle/\mathrm{d}y$, $\ell_\theta = \kappa_\theta y$ and $\kappa_\theta = \kappa/Pr_t$, where Pr_t is the turbulent Prandtl number. Consequently, the mean temperature gradient is written as follows:

$$\frac{\mathrm{d}\langle\theta\rangle}{\mathrm{d}y} = Pr_t\frac{\theta_\tau}{\kappa}\frac{(1+\beta_\theta y/H)}{y\,(1+\beta y/H)^{1/2}}. \tag{11}$$

Notice that the linear stress and heat flux assumptions are both valid for the fully developed thermal channel flow. From Eq. (11), the logarithmic law for the mean temperature, $\langle\theta\rangle^+ = (Pr_t/\kappa)\log y^+ + B_\theta$, is obtained provided that $|\beta y/H| \ll 1$ and $|\beta_\theta y/H| \ll 1$ with a constant turbulent Prandtl number. Eq. (11) is also rewritten as

$$\frac{\mathrm{d}\langle\theta\rangle}{\mathrm{d}y} = Pr_t\frac{\theta_\tau}{\kappa}\frac{1}{y}\left[1 + \frac{1}{2}(2\beta_\theta - \beta)\frac{y}{H} - \frac{1}{8}\beta(4\beta_\theta - 3\beta)\left(\frac{y}{H}\right)^2 + \cdots\right]. \tag{12}$$

Eq. (12) indicates that the mean temperature profile depends on both β and β_θ, while the mean velocity profile

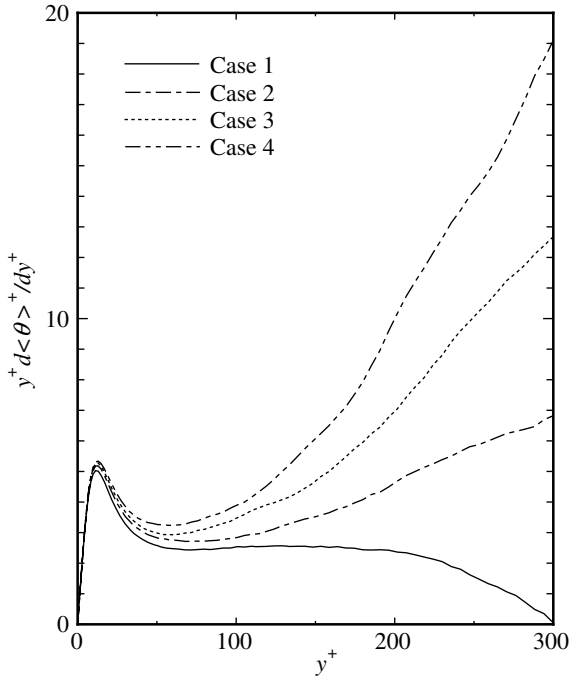

Fig. 5. Inspection of the logarithmic law of mean temperature: $y^+\mathrm{d}\langle\theta\rangle^+\,\mathrm{d}y^+$.

depends only on β (Eq. (10)), where the values of β and β_θ in the present DNS are presented in Table 1. The increase of the temperature gradient with increasing β_θ in Fig. 5 is explained by the additional terms in Eq. (12). The logarithmic temperature law seems to be appeared for Case 1 as shown in Fig. 5, while the logarithmic velocity law does not appear as shown in Fig. 4 under the present numerical conditions ($Re_\tau = 300$, $Pr = 0.72$). This difference would be attributed to the profile of the turbulent Prandtl number $Pr_t = \langle u_1' u_2' \rangle \mathrm{d}\langle\theta\rangle/\mathrm{d}y / (\langle u_2' \theta' \rangle \mathrm{d}\langle u_1 \rangle/\mathrm{d}y)$ shown in Fig. 6. Pr_t decreases with increasing y^+, and removes the bump of mean temperature profile for Case 1 in Fig. 5, which is produced by the additional terms in Eq. (12). Note that no logarithmic temperature law is observed for Cases 2, 3, and 4, which is due to the higher temperature on the opposite wall.

The above analysis (Eqs. (10) and (12)) implies that both apparent logarithmic velocity and temperature laws may appear for the case with $\beta = \beta_\theta = 0$ which corresponds to the thermal flow with zero heat flux gradient in pure Couette flow. For the further discussion on the logarithmic velocity and temperature laws, the experimental and numerical studies at the higher Reynolds number would be needed.

4.2. Turbulence statistics

The RMS temperature fluctuations (temperature variance) scaled by the friction temperature $(\theta')^+_{\mathrm{rms}} = (\theta')_{\mathrm{rms}}/\theta_\tau$ is shown in Fig. 7. The RMS velocity fluctuation is in good agreement with the corresponding DNS data [24] and is not shown here. The peak value of the temperature variance in the wall coordinate increases in order of Case 1 ($\beta_\theta = -1$), Case 2 ($\beta_\theta = -0.5$), Case 3 ($\beta_\theta = 0$), and Case 4 ($\beta_\theta = +0.5$), i.e., with increasing β_θ at $Re_\tau = 300$. And the difference in $(\theta')^+_{\mathrm{rms}}$ among cases is considerably large for $y^+ > 50$. This implies the possibility that the temperature fluctuation is well arranged by a proper temperature scale, which reflects the variation of β_θ. One of the candidates is the local friction temperature defined as $\theta_L = q_{\mathrm{total}}/(\rho c_{\mathrm{p}} u_L)$, where $u_L = \sqrt{\tau_{\mathrm{total}}/\rho}$ is the local friction velocity. Fig. 8 shows

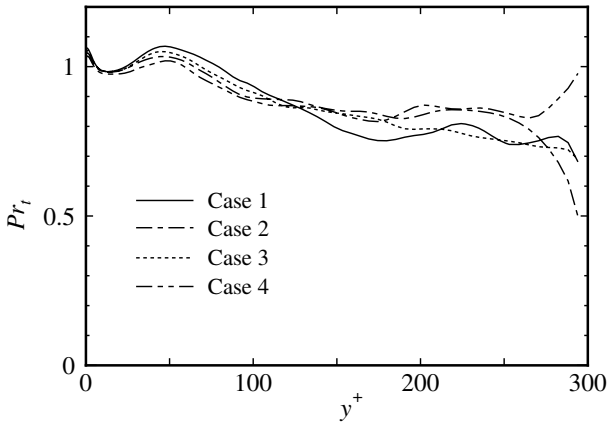

Fig. 6. Profiles of turbulent Prandtl number.

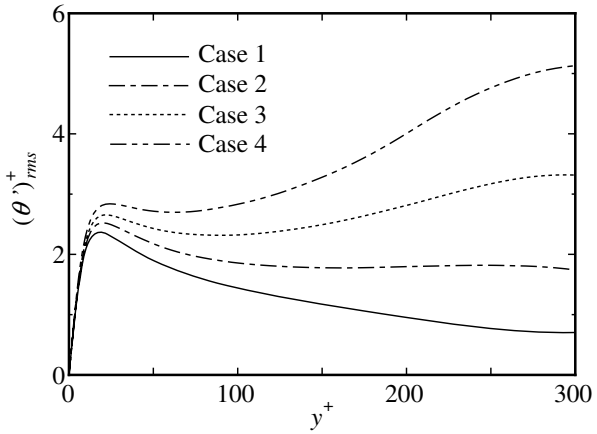

Fig. 7. Profiles of temperature variance in wall units.

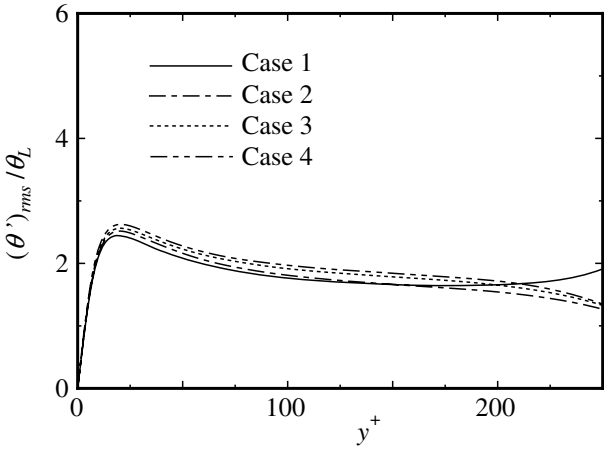

Fig. 8. Profiles of temperature variance normalized by local friction temperature.

temperature variance scaled by θ_L. It is noticeable that the temperature fluctuation intensity is well scaled by θ_L close to the lower wall at the same Reynolds number.

Fig. 9a and b show the profiles of streamwise turbulent heat flux $-\langle u_1'^+ \theta'^+ \rangle$ and $-\langle u_1'^+ \theta' \rangle/\theta_L$, respectively. Similar to the RMS temperature fluctuation, the streamwise turbulent heat flux is well scaled by using the local friction temperature θ_L, while $-\langle u_1'^+ \theta'^+ \rangle$ increases with increasing β_θ. Figs. 10a and b show the profiles of wall-normal turbulent heat flux $-\langle u_2'^+ \theta'^+ \rangle$ and $-\langle u_2'^+ \theta' \rangle/\theta_L$, respectively. The wall-normal turbulent heat flux scaled by the local friction temperature θ_L also collapses onto a single curve. This is analytically explained as follows. The wall-normal heat flux $-\langle u_2'^+ \theta' \rangle/\theta_L$ is given as

$$\frac{\langle u_2'^+ \theta' \rangle}{\theta_L} = \frac{\rho c_{\mathrm{p}}}{q^\ell + q^t} \sqrt{\frac{\tau^\ell + \tau^t}{\rho}} \frac{\langle u_2' \theta' \rangle}{u_\tau}. \tag{13}$$

In the turbulent region ($\tau^t \gg \tau^\ell$, $q^t \gg q^\ell$), Eq. (13) is rewritten as follows:

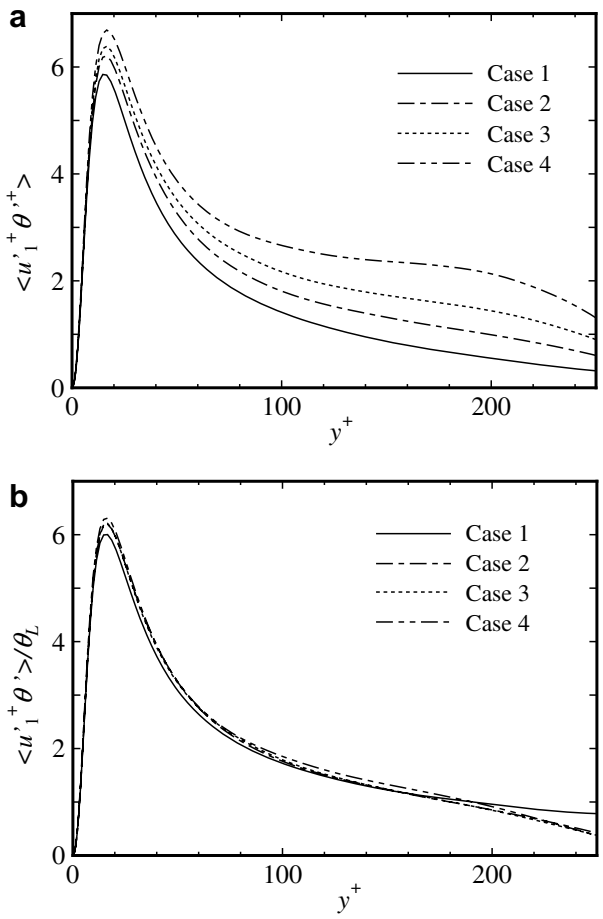

Fig. 9. Profiles of streamwise turbulent heat flux: (a) in wall units; (b) local scaling.

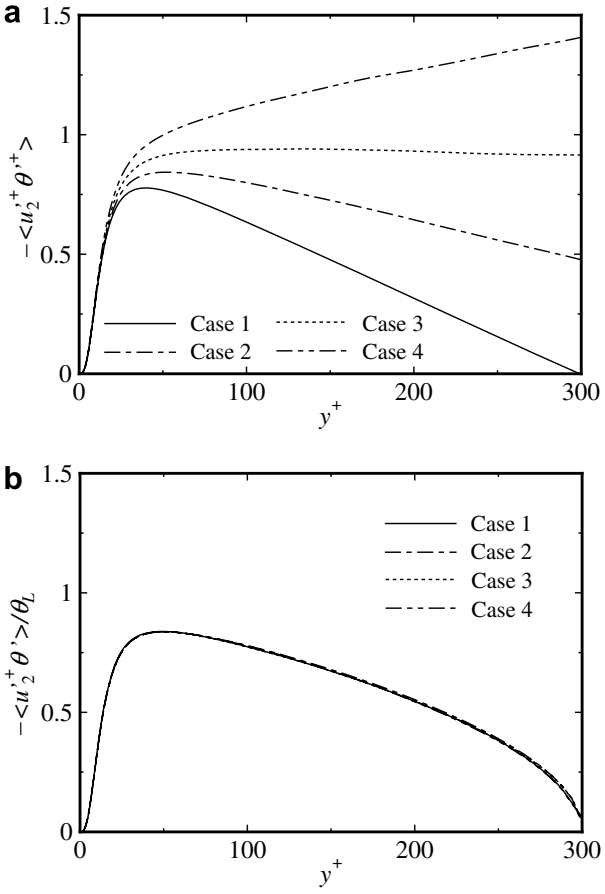

Fig. 10. Profiles of wall-normal turbulent heat flux: (a) in wall units; (b) local scaling.

$$\frac{\langle u_2'^+\theta'\rangle}{\theta_L}=\sqrt{\frac{\tau^t}{\tau_w}}. \tag{14}$$

Eq. (14) indicates that the profile of $\langle u_2'^+\theta'\rangle/\theta_L$ depends only on the velocity field and is the same for all the cases tested. Note that the anisotropy of the streamwise and wall-normal turbulent heat flux is not altered by total heat flux gradients as understood from Figs. 9b and 10b.

The budget data obtained by DNS are very helpful for understanding the detailed mechanism of the profiles of turbulence statistics such as temperature variance and heat fluxes. The transport equation of temperature variance $k_\theta^+=\langle\theta'^{+2}\rangle/2$ is

$$-\langle u_2'^+\theta'^+\rangle\frac{\mathrm{d}\langle\theta\rangle^+}{\mathrm{d}x_2^+}-\frac{1}{Pr}\left\langle\left(\frac{\partial\theta'^+}{\partial x_k^+}\right)^2\right\rangle-\frac{\partial\langle u_j'^+\theta'^{+2}/2\rangle}{\partial x_2^+}+\frac{1}{Pr}\frac{\mathrm{d}^2k_\theta^+}{\mathrm{d}x_2^{+2}}=0, \tag{15}$$

where the first to fourth terms are production P_θ^+, dissipation ε_θ^+, turbulent diffusion, and molecular diffusion, respectively. The transport equation of the dissipation rate of temperature variance ε_θ^+ is as follows:

$$\begin{aligned}
&-\frac{2}{Pr}\left[\left\langle\frac{\partial\theta'^+}{\partial x_k^+}\frac{\partial u_2'^+}{\partial x_k^+}\right\rangle\frac{\mathrm{d}\langle\theta\rangle^+}{\mathrm{d}x_2^+}+\left\langle\frac{\partial\theta'^+}{\partial x_k^+}\frac{\partial\theta'^+}{\partial x_k^+}\right\rangle\frac{\mathrm{d}\langle u_j\rangle^+}{\mathrm{d}x_k^+}\right]\\
&-\frac{2}{Pr}\left\langle u_2'^+\frac{\partial\theta'^+}{\partial x_2^+}\right\rangle\frac{\mathrm{d}^2\langle\theta\rangle^+}{\mathrm{d}x_2^+\mathrm{d}x_2^+}-\frac{2}{Pr}\left\langle\frac{\partial\theta'^+}{\partial x_k^+}\frac{\partial\theta'^+}{\partial x_j^+}\frac{\partial u_j'^+}{\partial x_k^+}\right\rangle\\
&-\frac{2}{Pr^2}\left\langle\left(\frac{\partial^2\theta'^+}{\partial x_k^+\partial x_k^+}\right)^2\right\rangle-\frac{1}{Pr}\frac{\mathrm{d}}{\mathrm{d}x_2^+}\left\langle u_2'^+\left(\frac{\partial\theta'^+}{\partial x_k^+}\right)^2\right\rangle\\
&+\frac{1}{Pr}\frac{\mathrm{d}^2\varepsilon_\theta^+}{\mathrm{d}x_2^{+2}}=0,
\end{aligned} \tag{16}$$

where the first to sixth terms are mean gradient production, gradient production, turbulent production, dissipation, turbulent diffusion, and molecular diffusion, respectively. The transport equation of turbulent heat flux $\langle u_i'^+\theta'^+\rangle$ is

$$\begin{aligned}
&-\langle u_i'^+u_2'^+\rangle\frac{\mathrm{d}\langle\theta\rangle^+}{\mathrm{d}x_2^+}-\langle u_2'^+\theta'^+\rangle\frac{\mathrm{d}\langle u_i\rangle^+}{\mathrm{d}x_2^+}\\
&-\left(1+\frac{1}{Pr}\right)\left\langle\frac{\partial u_i'^+}{\partial x_j^+}\frac{\partial\theta'^+}{\partial x_j^+}\right\rangle+\left\langle p'^+\frac{\partial\theta'^+}{\partial x_i^+}\right\rangle-\frac{\mathrm{d}\langle p'^+\theta'^+\rangle}{\mathrm{d}x_i^+}\\
&-\frac{\mathrm{d}\langle u_i'^+u_2'^+\theta'^+\rangle}{\mathrm{d}x_2^+}+\frac{\mathrm{d}}{\mathrm{d}x_2^+}\left[\frac{1}{Pr}\left\langle u_i'^+\frac{\partial\theta'^+}{\partial x_2^+}\right\rangle+\left\langle\theta'^+\frac{\partial u_i'^+}{\partial x_2^+}\right\rangle\right]=0,
\end{aligned} \tag{17}$$

where the first to sixth terms are production, dissipation, pressure temperature-gradient correlation, pressure diffusion, turbulent diffusion, and molecular diffusion, respectively.

The budgets for Cases 1 and 3 agree well with existing DNS data [3,12]. The budget profiles for k_θ and ε_θ of Cases 1 and 3 are symmetric with respect to the center of the channel. The profiles of $\langle u_1'\theta'\rangle$ for Cases 1 and 3 are symmetric and anti-symmetric, respectively, while the profiles of $\langle u_2'\theta'\rangle$ for Cases 1 and 3 are anti-symmetric and symmetric, respectively. The budget for Case 2 seems to be the same as that of the lower half for Case 1, and the temperature variance and turbulence heat flux generations are small close to the upper wall. For simplicity, detailed budgets for Cases 1, 2 and 3 are omitted here. The budgets of the temperature variance, its dissipation rate, streamwise and wall-normal turbulent heat fluxes are presented in Fig. 11a–d, respectively, for Case 4 as a representative. Although the terms in the budgets near the upper wall are larger than those near the lower wall for Case 4, the upper and lower profiles agree well with each other when they are normalized by the corresponding wall variables.

In the budget of k_θ, the production term P_θ^+ increases with increasing β_θ on the lower wall side and balances with the dissipation term ε_θ^+ as shown in Fig. 12a and b. The main terms in the budget of ε_θ are the mean gradient production, turbulent production, and dissipation terms as shown in Fig. 11b, and their amplitudes increase with increasing β_θ (not shown here).

In the wall-normal turbulent heat flux balance, the production term $P_{2\theta}^+$ and the pressure temperature-gradient correlation term $PTG_{2\theta}^+$ are balanced as shown in Fig. 13a and b. In addition, the amplitudes of the pressure diffusion term $PD_{2\theta}^+$ and the turbulent diffusion term $TD_{2\theta}^+$ increase with increasing the total heat flux gradient, and they balance with each other at the central region of the channel as shown in Figs. 14a and b.

The production terms of temperature variance and wall-normal turbulent heat flux scaled by the local friction temperature, $P_\theta^{+L} = P_\theta/(u_\tau\theta_L^2/\delta_v)$ and $P_{2\theta}^{+L} = P_{2\theta}/(u_\tau^2\theta_L/\delta_v)$, are presented in Figs. 15a and b, respectively. It can be found that the production terms P_θ^{+L} and $P_{2\theta}^{+L}$ do not vary with β_θ, which supports the usefulness of the new scaling using the local friction temperature θ_L.

5. Conclusions

The new scaling of turbulence statistics for wall-bounded thermal turbulent flow with different total heat flux gradients was investigated using direct numerical simulation (DNS) of the incompressible turbulent channel flow with passive scalar transport at $Re_\tau = 300$ and $Pr = 0.72$. DNS for four cases were performed, where the non-dimensional wall-normal gradients of the total heat flux β_θ are -1, -0.5, 0 and $+0.5$. The dependence of β_θ on the turbulence statistics is discussed using the DNS data. Temperature variance and turbulent heat flux were well scaled by the local friction temperature θ_L at the same Reynolds number. This finding was supported by the profiles of the

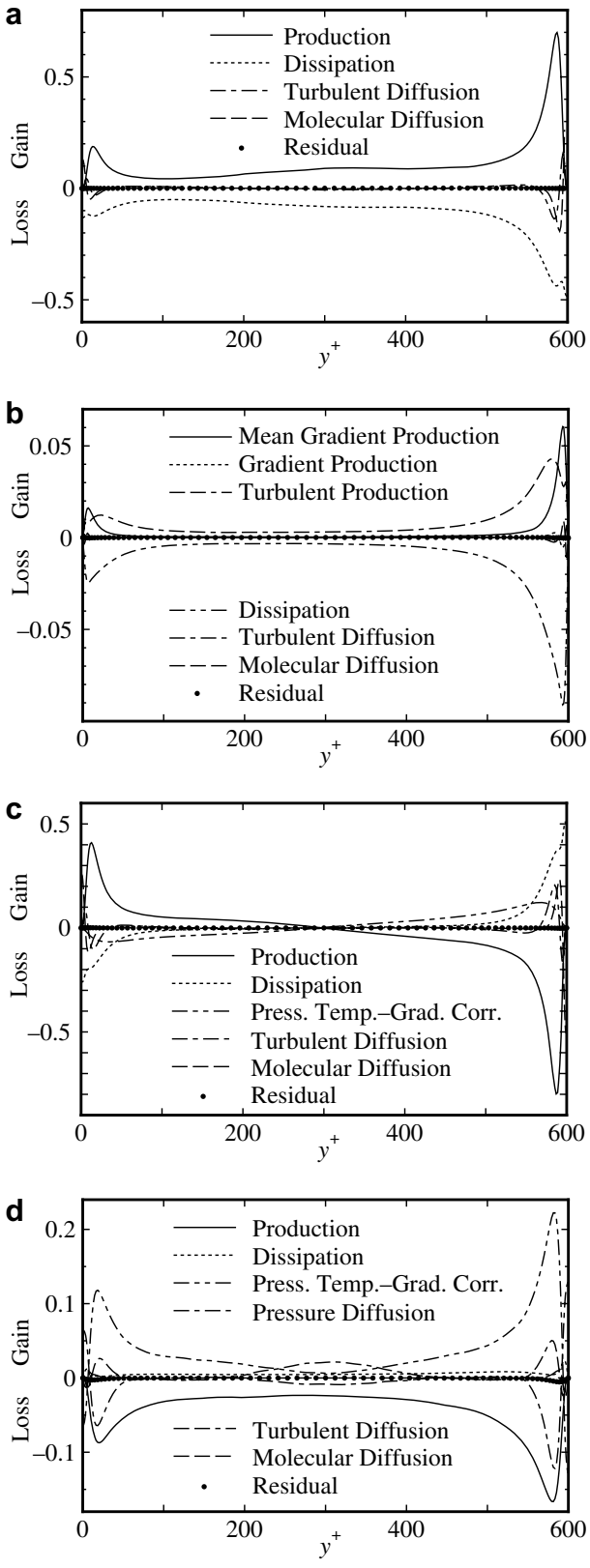

Fig. 11. Budgets of: (a) temperature variance k_θ^+; (b) dissipation for temperature variance ε_θ^+; (c) streamwise turbulence heat flux $\langle u_1'^+\theta'^+\rangle$; (d) wall-normal turbulence heat flux $\langle u_2'^+\theta'^+\rangle$ for Case 4.

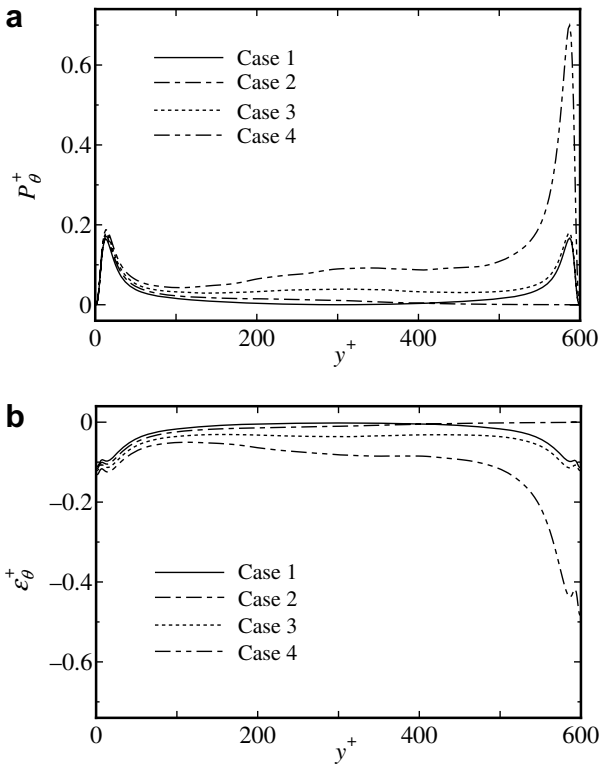

Fig. 12. Production and dissipation terms in k_θ^+ budget: (a) production term; (b) dissipation term.

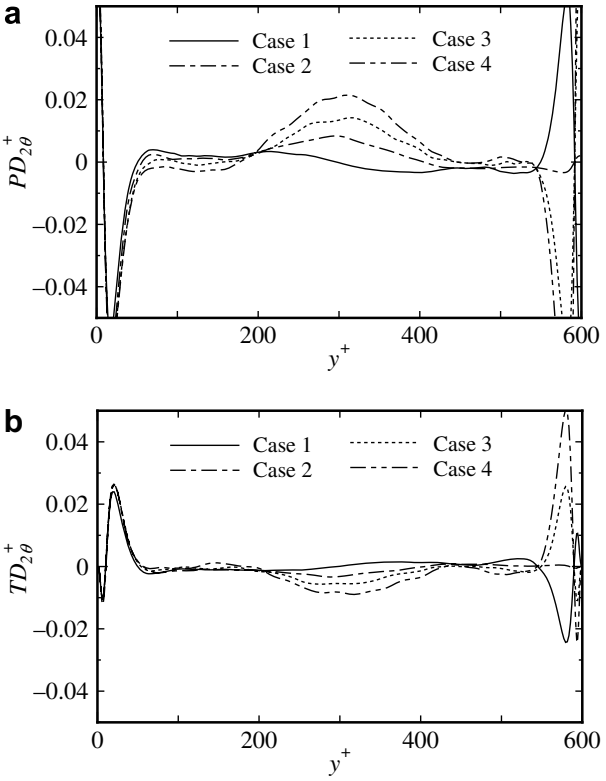

Fig. 14. Pressure diffusion and turbulent diffusion terms in $\langle u_2'^+\theta'^+\rangle$ budget: (a) pressure diffusion term; (b) turbulent diffusion term.

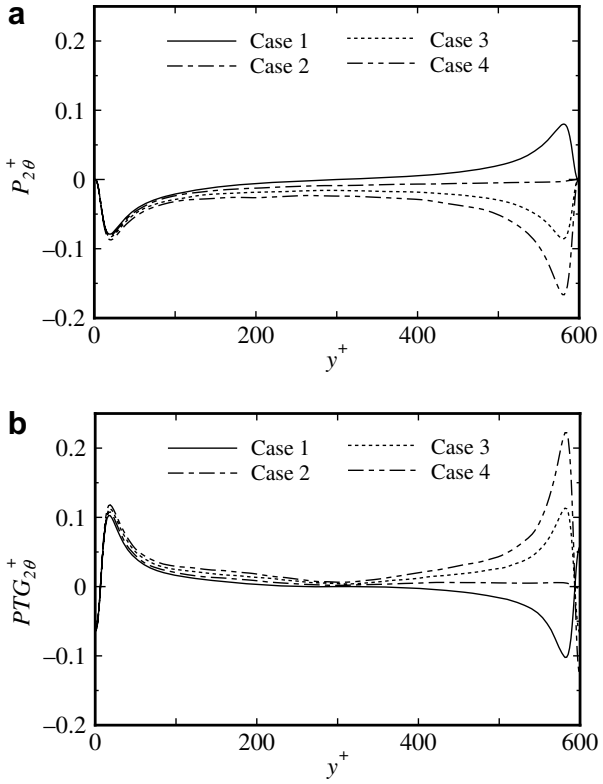

Fig. 13. Production and pressure temperature-gradient correlation terms in $\langle u_2'^+\theta'^+\rangle$ budget: (a) production term; (b) pressure temperature-gradient correlation term.

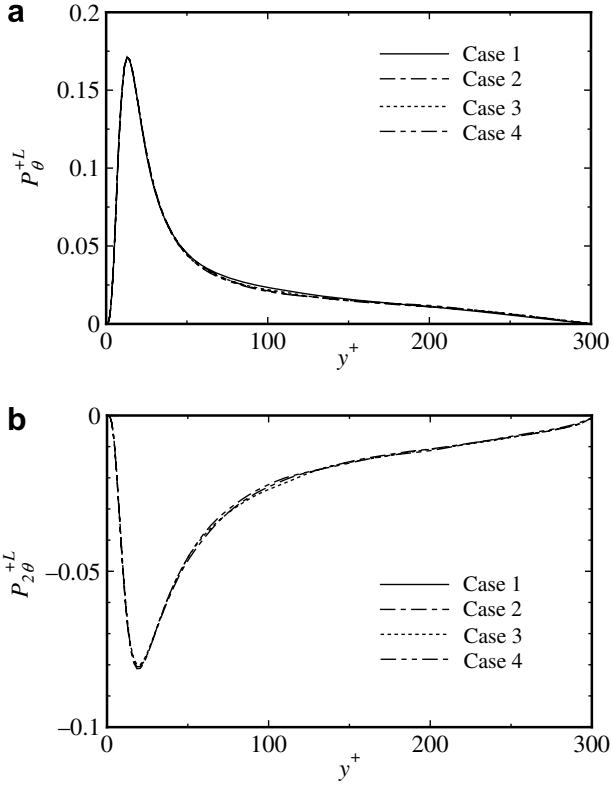

Fig. 15. Production terms of temperature variance and wall-normal turbulent heat flux scaled by θ_L: (a) $P_\theta^{+L} = P_\theta/(u_\tau\theta_L^2/\delta_v)$; (b) $P_{2\theta}^{+L} = P_{2\theta}/(u_\tau^2\theta_L/\delta_v)$.

corresponding production terms. The production and dissipation terms are balanced in the budgets of k_θ and ε_θ. In the budget of the wall-normal turbulent heat flux $\langle u_2'\theta'\rangle$, the production term and the pressure temperature-gradient correlation term are balanced. An additional balance is also observed between the pressure diffusion and turbulent diffusion terms in the budget of $\langle u_2'\theta'\rangle$. The amplitudes of balanced terms increase with increasing β_θ. In addition, using the linear stress-heat flux model presented here, it is shown that the appearance of the logarithmic temperature profile is attributed to the distribution of the turbulent Prandtl number, while the logarithmic velocity law does not appear.

Acknowledgements

The computations performed on a Fujitsu VPP5000 and a Hitachi SR8000 at the Center for Promotion of Computational Science and Engineering, Japan Atomic Energy Research Institute, are gratefully acknowledged. Y.M. was partially supported by a Grant-in-Aid for Scientific Research (No. 17656066 and No. 18360087) from Japan Society for Promotion of Science.

References

[1] J. Kim, P. Moin, Transport of passive scalar in a turbulent channel flow, Turbulent Shear Flows VI, Springer, Berlin, 1989, pp. 85–96.
[2] S.L. Lyons, T.J. Hanratty, J.B. McLaughlin, Direct numerical simulation of passive heat transfer in a turbulent channel flow, Int. J. Heat Mass Transfer 34 (1991) 1149–1161.
[3] N. Kasagi, Y. Tomita, A. Kuroda, Direct numerical simulation of passive scalar field in a turbulent channel flow, J. Heat Transfer 144 (1992) 598–606.
[4] K. Horiuti, Assessment of two-equation models of turbulent passive-scalar diffusion in channel flow, J. Fluid Mech. 238 (1992) 405–433.
[5] M. Teitel, R.A. Antonia, Heat transfer in fully developed turbulent channel flow: comparison between experiment and direct numerical simulations, Int. J. Heat Mass Transfer 36 (1993) 1701–1706.
[6] H. Kawamura, K. Ohsaka, H. Abe, K. Yamamoto, DNS of turbulent heat transfer in channel flow with low to medium-high Prandtl number fluid, Int. J. Heat Fluid Flow 19 (1998) 482–491.
[7] A.V. Johansson, P.M. Wikström, DNS and modeling of passive scalar transport in turbulent channel flow with a focus on scalar dissipation rate modeling, Flow Turbul. Combust. 63 (1999) 223–245.
[8] H. Kong, H. Choi, J.S. Lee, Direct numerical simulation of turbulent thermal boundary layers, Phys. Fluids 12 (2000) 2555–2568.
[9] Y. Na, T.J. Hanratty, Limiting behavior of turbulent scalar transport close to a wall, Int. J. Heat Mass Transfer 43 (2000) 1749–1758.
[10] I. Tiselj, R. Bergant, B. Mavko, I. Bajsić, G. Hetsroni, DNS of turbulent heat transfer in channel flow with heat conduction in the solid wall, J. Heat Transfer 123 (2001) 849–857.
[11] I. Tiselj, E. Pogrebnyak, C. Li, A. Mosyak, G. Hetsroni, Effect of wall boundary condition on scalar transfer in a fully developed turbulent flume, Phys. Fluids 13 (2001) 1028–1039.
[12] O. Iida, N. Kasagi, Y. Nagano, Direct numerical simulation of turbulent channel flow under stable density stratification, Int. J. Heat Mass Transfer 45 (2002) 1693–1703.
[13] H. Abe, H. Kawamura, Y. Matsuo, Surface heat-flux fluctuations in a turbulent channel flow up to $Re_\tau = 1020$ with $Pr = 0.025$ and 0.71, Int. J. Heat Fluid Flow 25 (2004) 404–419.
[14] L. Kleiser, U. Schumann, Treatment of incompressibility and boundary conditions in 3-D numerical spectral simulations of plane channel flows, in: E.H. Hirschel (Ed.), Proceedings of the Third GAMM Conference on Numerical Methods in Fluid Mechanics, Vieweg, Brauschweig, 1980, pp. 165–173.
[15] J. Werne, Incompressibility and no-slip boundaries in the Chebyshev-tau approximation: Correction to Kleiserand Schumann's influence-matrix solution, J. Comput. Phys. 120 (1995) 260–265.
[16] A.G. Kravchenko, P. Moin, On the effect of numerical errors in large eddy simulations of turbulent flows, J. Comput. Phys. 131 (1997) 310–322.
[17] A.A. Wray, Minimal storage time-advancement schemes for spectral methods, NASA-Ames Research Center, Moffett Field, CA, private communication, 1986.
[18] P.R. Spalart, R.D. Moser, M.M. Rogers, Spectral methods for the Navier–Stokes equations with one infinite and two periodic directions, J. Comput. Phys. 96 (1991) 297–324.
[19] C. Canuto, M. Hussaini, A. Quarteroni, T. Zang, Spectral Methods in Fluid Dynamics, Springer, Berlin, 1988.
[20] Y. Morinishi, S. Tamano, K. Nakabayashi, Direct numerical simulation of compressible turbulent channel flow between adiabatic and isothermal walls, J. Fluid Mech. 502 (2004) 273–308.
[21] Y. Morinishi, S. Tamano, E. Nakamura, Numerical analysis of incompressible turbulent channel flow with different thermal wall boundary conditions, Trans. JSME, Ser. B 69 (2003) 1313–1320 (in Japanese).
[22] D.B. Spalding, On similarity solutions for free-convection flow past flat plates, J. Appl. Mech. 23 (1961) 455–458.
[23] A.A. Townsend, Equilibrium layers and wall turbulence, J. Fluid Mech. 11 (1960) 97–120.
[24] K. Iwamoto, Y. Suzuki, N. Kasagi, Reynolds number effect on wall turbulence: toward effective feedback control, Int. J. Heat Fluid Flow 23 (2002) 678–689.
[25] M.V. Zagarola, A.J. Smits, Mean-flow scaling of turbulent pipe flow, J. Fluid Mech. 373 (1998) 33–79.